Numerical Analysis of a Supercritical Heat Transfer of Cryogenic Methane in Regeneratively Cooled Rocket Engine

Mohammed Amine DJEFFAL*,[1], Nabil BENAMARA[1], Abdelkader LAHCENE[1], Ali BENOUAR[2], Abdelkader BOULENOUAR[1], Mohammed MERZOUG[1]

*Corresponding author
[1]Laboratory of Materials and Reactive Systems (LMSR),
Mechanical Engineering Department, Djillali Liabes University,
City Larbi Ben Mhidi, P.O. Box 89, 22000 Sidi Bel Abbes, Algeria,
djeffalmohammed66@gmail.com*, mohammed.djeffal@univ-sba.dz
[2]Laboratory of complex systems (LCS),
Higher School of Electrical and Energy Engineering ESGEE,
Oran, Algeria

DOI: 10.13111/2066-8201.2024.16.1.4

Received: 11 January 2024/ Accepted: 12 February 2024/ Published: March 2024

Abstract: *A comparative study of supercritical heat transfer in a regeneratively cooled rocket engine was conducted using three-dimensional numerical simulations for two channel geometries: rectangular and square. Various constant heat fluxes, flow velocities, and operating pressures were imposed to study their effect on heat transfer, pressure losses, and the conditions under which heat transfer deterioration HTD occurs. The results show that a rectangular channel is more efficient in terms of heat transfer than a square channel, with a more pronounced difference at high heat fluxes and low velocities, these conditions, in fact, favored the occurrence of heat transfer deterioration, particularly in the square channel. Increasing the flow velocities to reduce the wall temperature and prevent thermal deterioration was accompanied by a significant increase in pressure losses, these pressure losses are greater in the rectangular channel, despite its advantages in terms of heat transfer. Operating pressure also plays an important role in heat transfer, increasing the pressure results in a decrease in wall temperature.*

Key Words: *Regenerative cooling, Supercritical pressure Methane, Heat transfer deterioration, Liquid propellant rocket engines*

1. INTRODUCTION

Regenerative cooling is an efficient and inevitable cooling technique for liquid-propellant rocket engines LPREs with high thrust and long burn duration [1]. This system uses the engine's own propellant, typically the fuel, as the coolant. It enters the cooling channels and, as it circulates, absorbs the heat released by the combustion process. It is then injected into the combustion chamber, where it is mixed with the oxidizer and burned. This cooling process helps to maintain the combustion chamber temperature at an optimal level.

In the early days, with the engines of the V2 missile and other improved versions of the same engine, the double-wall configuration made of welded sheet metal was used. However,

as the engines went to higher thrust levels, this configuration quickly reached its limits and was abandoned. This was because the very thin walls were no longer able to withstand high pressures, while walls that were thick enough to resist buckling would have insufficient heat transfer. This led to the development of other types of construction, such as tubular design, which were widely adopted by several manufacturers. The tubes were brazed together by hand or in furnaces. However, more recently, as engines have become increasingly efficient and require even higher pressures, channel wall or sandwich wall designs have become the most common type of construction. In this type, the inner liner with channels form is brazed to the close-out wall [2]. Several studies have investigated the influence of the height-to-width aspect ratio of rectangular channel walls on the heat transfer efficiency in LPREs [3–6]. In the study of A. Ulas and E. Boysan [7] in particular, the researchers conducted numerical simulations and were able to determine that increasing the height-to-width aspect ratio improves heat transfer but also results in higher pressure losses. In addition, they found that with an optimal number of channels and a variation of the cross-section along the engine axis, it was possible to achieve acceptable wall temperatures while significantly reducing pressure losses.

The objective of this research is to study the influence of constant heat fluxes, operation pressures and the inlet velocities on the heat transfer efficiency of two channels with the same surface area with different cross-sectional aspect ratios, a square (Sqr) and a rectangular (Rec) channel. Using methane as a coolant. Indeed, the use of liquid methane as a fuel for LPREs has recently attracted growing interest [8–10], given its many advantages compared to other propellants, making it a very good choice for the new generation of liquid-fueled rocket engines. Methane combines and presents a good balance of properties. Indeed, it offers good performance, with a high specific impulse, a high density and therefore small tanks to store it, a high boiling point, high coking limit, it can be synthesized on other planets, and it has good cooling capacity.

In LPREs, methane is most often injected into the cooling channels at a pressure above its critical pressure. As it circulates through the channels, its temperature increases. However, it will not undergo a phase transition during its passage but at a certain temperature called pseudo-critical temperature, methane will change from a liquid-like to a gas-like state. This change of state is accompanied by a drastic increase in the specific heat of methane. While the density, thermal conductivity, and dynamic viscosity of methane decrease. The pressure also has an influence on the thermophysical properties of methane. As the pressure increases, the change in these properties becomes less pronounced. as shown in Fig. 1. Many research has been conducted on supercritical fluids to improve the design of air conditioning and refrigeration systems, steam boilers, nuclear reactors, and supercritical reactors [11–13]. These studies have shown that the ratio of heat flux to mass flux plays a critical role in heat transfer. In fact, at high values of this ratio, heat transfer can deteriorate due to phenomena such as laminarization of the flow near the heated wall and thermal stratification. In the region where the bulk temperature is below the pseudo-critical temperature and the near wall temperature is above this temperature, separation can occur between the hot fluid, close to the gaseous state, near the wall and the cold fluid, close to the liquid state, in the bulk. This separation can lead to a heat transfer deterioration HTD and a dangerous increase in wall temperatures.

Younglove and Ely [14] studied the thermophysical properties of several fluids including methane at different supercritical pressures. Ya-Zhou Wang et al. [15] conducted numerical studies of turbulent convective heat transfer of cryogenic methane flowing inside a horizontal minitube under supercritical pressures for rocket propulsion applications. They concluded that higher operating pressures for methane can generally improve heat transfer, especially at high heat fluxes, and existing formulas such as Gnielinski's do not work well as they cannot handle

the drastic property changes at supercritical pressures of methane. They established a modified expression for supercritical heat transfer for better predictions, showing very good accuracy except when the pressure is below 8 MPa and the heat flux is greater than 7 MW/m². Bo Ruan and Hua Meng [16] studied supercritical turbulent heat transfer of methane in rectangular combustion chambers. They found in their three-dimensional numerical analysis that HTD occurs at low pressure and/or high wall heat flux. They also showed that a shallow cooling channel is effective for supercritical heat transfer, but it suffers a significant pressure loss. They also showed that Bishop's heat transfer equation [17] is applicable to supercritical cryogenic methane. Hungfang Gu et al. [18] studied supercritical heat transfer of methane in a horizontal miniature tube and proposed a new correlation based on the probability density function (PDF) for supercritical cryogenic methane that works well with over 85% of the experimental data. Pizzarelli and Battista [19] reviewed and assessed experimental studies on heat transfer in thrust chambers using methane and oxygen as propellants.

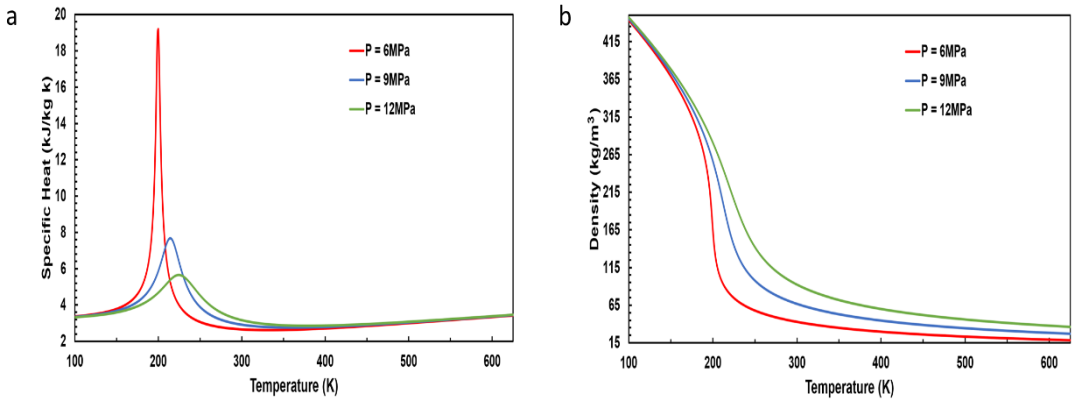

Fig. 1 - Specific heat (a) and density (b), of Methane at different supercritical pressures

2. MODELLING AND SIMULATION

The objective of this research is to study the influence of constant heat flux, operation pressure, and methane inlet velocity on forced convection heat transfer on two channels with different passage geometries. The material used in this study is copper alloy, with a width and height of 14 mm and 6 mm respectively, contains in its interior either a rectangular (Rec) or the square (Sqr) shape passage, i.e. different aspect ratio, both have a surface area A of 16 mm² (8x2 and 4x4 mm as height and width respectively for rectangular and square shape). The length of the two channels L of 300 mm typically equivalent to a combustion chamber length, heated on its bottom surface, as shown in Fig. 2. The internal wall thickness is 1 mm for both channels to ensure good heat transfer. Two 150 mm long fluid flow sections were added to allow for a fully developed flow at the inlet and to avoid the effect of the boundary condition at the outlet. Due to symmetry, only half of the channel along the z-plane is used in the numerical calculation.

The inlet temperature of the channels Ti is 120 K. Numerous simulations with different constant heat fluxes (asymmetric heating on the bottom surface of the material) and inlet velocities to study their effect on heat transfer have been carried out as follows: q'' of 2, 3.5 and 5 MW/m², and inlet velocities u_∞ of 5, 10 and 15 m/s. Also, to study the effect of operation pressure, with the inlet velocity of u_∞ = 15 m/s, three outlet pressures Pe were simulated: 6, 9 and 12 MPa with the different heat fluxes mentioned above. The properties of methane are

taken from the NIST database [20]. The variation of the thermal conductivity k of copper is taken from Simon et al. [21], integrated as Piecewise function.

For this three-dimensional numerical study, the ANSYS-Fluent 18.1 software was used. The fluid flow and heat transfer in the cooling channel were assumed to be stationary and turbulent. Tetrahedral elements were applied to the entire domain (solid and fluid). The resolution of the boundary layer near the walls was optimized using the Inflation in the meshing option. The k-ε turbulent model with an enhanced wall treatment was applied to accurately capture the strong temperature gradient, especially in the near-wall region. The continuity, momentum, and energy equations in the x, y et z directions describing the flow, and transport equations [22–24], are expressed below.

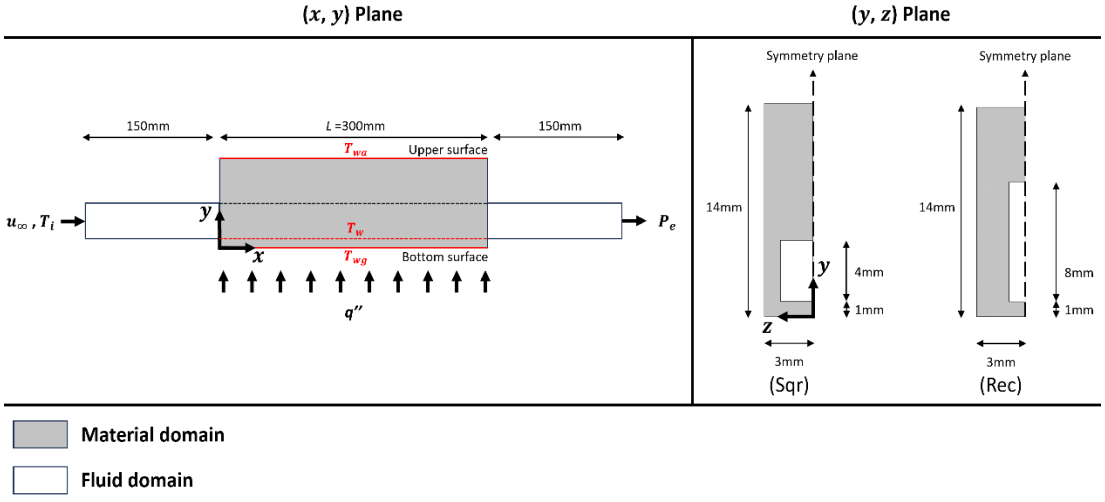

Fig. 2 - Schematic view of the solution domain

Continuity equation

$$\frac{\partial(\rho u_i)}{\partial x_i} = 0 \tag{1}$$

Momentum equation

$$\frac{\partial(\rho u_i)}{\partial t} + \frac{\partial(\rho u_i u_j)}{\partial x_j} = -\frac{\partial P}{\partial x_i} + \frac{\partial}{\partial x_j}\left[\mu\frac{\partial(u_i)}{\partial x_j} - \overline{\rho u'_i u'_j}\right] \tag{2}$$

Energy equation

$$\frac{\partial}{\partial x_i}(\rho T) + \frac{\partial}{\partial x_i}(\rho u_i T) = \frac{\partial}{\partial x_i}\left[\frac{k}{C_p}\frac{\partial T}{\partial x_i}\right] \tag{3}$$

Transport equations in k-ε model

$$\frac{\partial}{\partial t}(\rho k) + \frac{\partial}{\partial x_i}(\rho k u_i) = \frac{\partial}{\partial x_j}\left[\left(\mu + \frac{\mu_t}{\sigma_k}\right)\frac{\partial k}{\partial x_j}\right] + G_k + G_b - \rho\varepsilon - Y_M + S_k \tag{4}$$

and

$$\frac{\partial}{\partial t}(\rho\varepsilon) + \frac{\partial}{\partial x_i}(\rho\varepsilon u_i) = \frac{\partial}{\partial x_j}\left[\left(\mu + \frac{\mu_t}{\sigma_\varepsilon}\right)\frac{\partial \varepsilon}{\partial x_j}\right] + \rho C_1 S\varepsilon - \rho C_2 \frac{\varepsilon^2}{k + \sqrt{\nu\varepsilon}} + C_{1\varepsilon}\frac{\varepsilon}{k}C_{3\varepsilon}G_b + S_\varepsilon \tag{5}$$

where

$$C_1 = \max\left[0.43, \frac{\eta}{5+\eta}\right], \quad \eta = S\frac{k}{\varepsilon}, \quad S = \sqrt{2S_{ij}S_{ij}}$$

Turbulent viscosity

$$u_t = \rho\frac{k^2}{\varepsilon}\left[\frac{1}{4.04 + \sqrt{6}\frac{kU^*}{\varepsilon}\cos\varphi}\right] \tag{6}$$

where

$$U^* = \sqrt{S_{ij}S_{ij} + \acute{\Omega}_{ij}\acute{\Omega}_{ij}}, \quad \acute{\Omega}_{ij} = \Omega_{ij} - 2\varepsilon_{ijk}\omega_k, \quad \Omega_{ij} = \overline{\Omega_{ij}} - \varepsilon_{ijk}\omega_k, \quad \varphi = \frac{1}{3}\cos^{-1}\left(\sqrt{6}\Psi\right),$$

and

$$\Psi = \frac{S_{ij}S_{jk}S_{ki}}{S^{3}}, \qquad S = \sqrt{S_{ij}S_{ij}}, \qquad S_{ij} = \frac{1}{2}\left(\frac{\partial U_j}{\partial x_i} + \frac{\partial U_i}{\partial x_j}\right)$$

with

$$C_{1\varepsilon} = 1.44, \qquad C_2 = 1.9, \qquad \sigma_k = 1.0, \qquad \text{and } \sigma_\varepsilon = 1.2$$

Note:

In Continuity, Momentum and Energy equations, ρ is the density of fluid and u_i and u_j are the velocity component in the x, y and z coordinates. u_j is the velocity component in the x, y and z coordinates. μ is the viscosity and u' the velocity component fluctuation, therefore $\overline{\rho u'_i u'_j}$ is the turbulent stress. t is the time, and P is the pressure. T is the temperature, C_p is the specific heat, and k is the thermal conductivity.

In transport equations, G_k represents the generation of turbulence kinetic energy due to the mean velocity gradients, G_b is the generation of turbulence kinetic energy due to buoyancy, Y_M represents the contribution of the fluctuating dilatation in compressible turbulence to the overall dissipation rate, C_2 and $C_{1\varepsilon}$ are constants. σ_k and σ_ε are the turbulent Prandtl numbers for k and ε, respectively. S_k and S_ε are user-defined source terms.

In turbulent viscosity, $\overline{\Omega_{ij}}$ is the mean rate of rotation tensor viewed in a rotating reference frame with the angular velocity ω_k.

3. VALIDATION OF THE SOLVER

The model validation was performed using the numerical studies of turbulent convection heat transfer of cryogenic methane flowing inside a horizontal mini-tube of a rocket engine under supercritical pressures by Ya-Zhou Wang et al. [15].

Their channel has a diameter of 2 mm and a length L = 300 mm, exposed to a constant heat flux, and also as for our study, includes two non-heated sections of 150 mm each at the inlet and outlet of the channel to obtain a fully developed flow field at the beginning and avoid the effects of the boundary conditions at the outlet. The boundary conditions used for this validation are as follows: Ti = 120 K, u_∞= 25 m/s, and q'' = 3 MW/m².

Fig. 3 presents the results obtained from this validation, compared to the study by Ya-Zhou Wang et al.

The two graphs show good agreement between the two numerical simulations, with a maximum difference of 1.2% with the bulk temperature T_b and 1.8% with the wall temperature T_w.

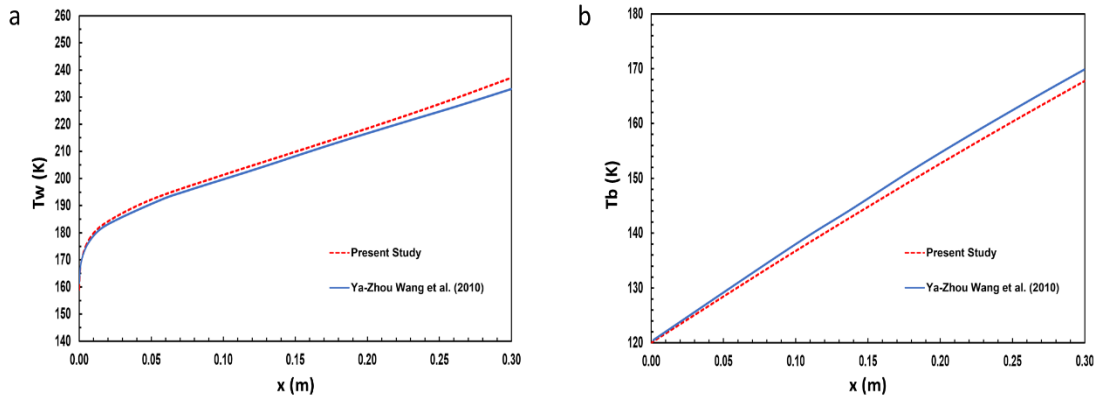

Fig. 3 - Variations along the engine x-axis in the wall temperature (a), and the fluid bulk temperature (b)

4. GRID CONVERGENCE

To obtain mesh-independent solutions, we studied the variation of the maximum bottom wall temperature T_{wg}, as a function of several grid element sizes, to find the size where T_{wg} converged, minimizing calculation time without sacrificing accuracy.

As shown in Fig. 4 and Table 1, we found that the solution converged with a grid element size of 4 × 10^-04 m, which corresponds to a number of elements of 1.83E+06. This element size was therefore chosen for the rest of the simulations.

Note: This study was conducted for the square channel, with an inlet velocity u_∞= 15 m/s, a constant heat flux q'' = 2 MW/m², and an outlet pressure Pe of 6 MPa.

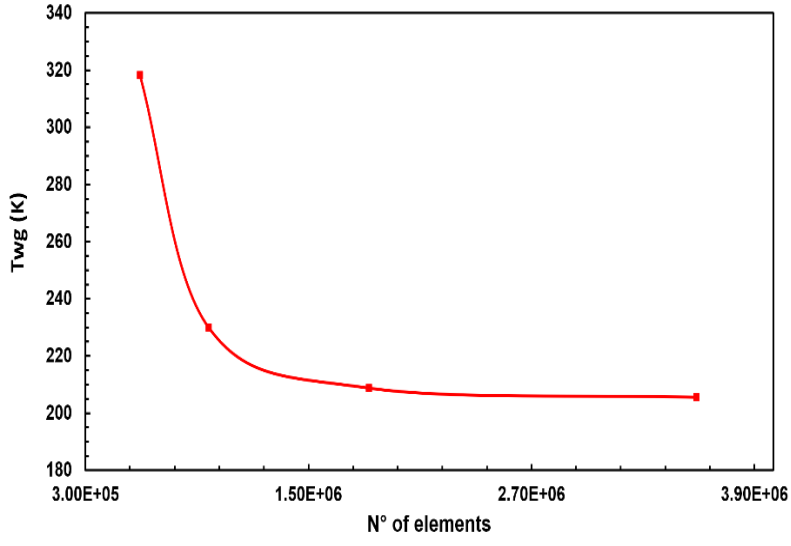

Fig. 4 - Convergence of the maximum wall temperature

Table 1 - Effect of grid element size on maximum wall temperature:

Grid elements size (m)	N° of elements	Maximum T_{wg} (K)	T_{wg} (%)
0.0006	592751	318.23	-
0.0005	963900	229.89	27.76

0.0004	1826176	208.82	9.17
0.0003	3587840	205.61	1.54

5. RESULTS AND DISCUSSIONS

5.1 Difference between heat transfer in a rectangular and square channel

In the first part of the study, we explored the impact of varying heat flux and inlet velocity on heat transfer in both rectangular and square channels while maintaining a constant operating pressure *Pe* at 9 MPa.

Our findings, presented in Table 2 and Fig. 7, revealed a better heat transfer performance in a rectangular channel which has a higher aspect ratio.

This difference is more pronounced with high heat fluxes and low velocities, and less noticeable with low heat fluxes and high velocities.

An example of this difference is illustrated in Fig. 5, which shows the temperature distribution at different positions along the x-axis of each channel for a constant heat flux q'' of 5 MW/m² and an inlet velocity u_∞ of 5 m/s.

In fact, with a heat flux q'' of 5 MW/m² and an inlet velocity u_∞ of 5 m/s, the difference in wall temperature facing the heat flux T_{wg} (bottom surface) between the two channels reaches more than 35.2%, and more than 40.1% in the adiabatic wall T_{wa} (upper surface).

This difference in heat transfer between the two channels, especially with high velocities, is due to the fact that a rectangular channel tends to favor a more turbulent flow.

his type of flow allows the coolant to mix more effectively, thereby improving heat transfer. Fig. 6 shows the difference in turbulent kinetic energy between the two channels at u_∞= 5 m/s with a heat flux q'' = 5 MW/m².

It is noted that the turbulent kinetic energy is higher in the rectangular channel, especially near the fluid-wall contact surface, with a maximum value of 6.54 m²/s² for the rectangular channel and only 2.83 m²/s² for the square channel.

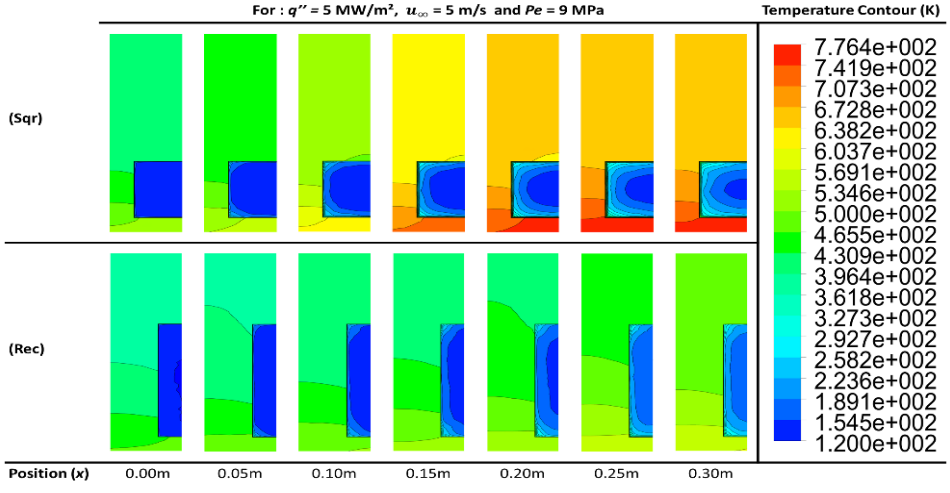

Fig. 5 - Temperature distribution along the x-axis of each channel for a constant heat flux q'' of 5 MW/m² and an inlet velocity u_∞ of 5 m/s, at the operating outlet pressure *Pe* of 9 MPa

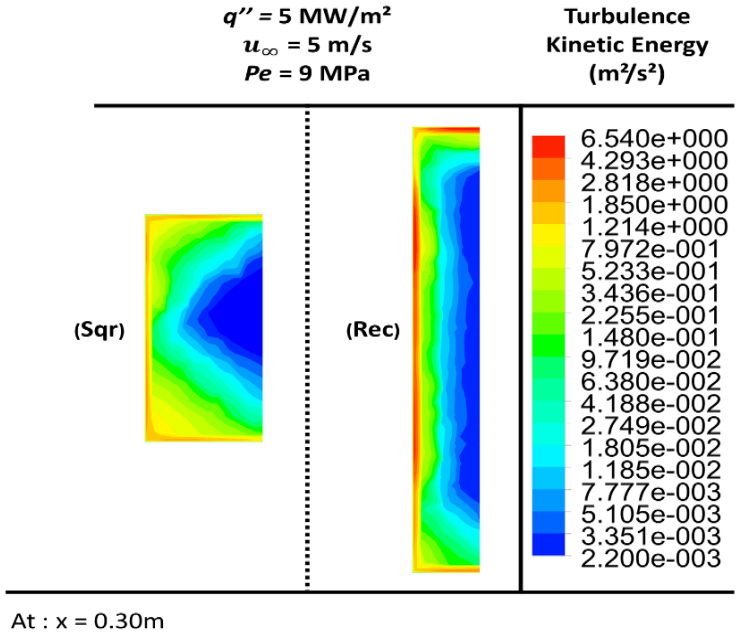

Fig. 6 - Turbulent kinetic energy distribution for the square and the rectangular channels at the outlet, for q'' = 5 MW/m² and an inlet velocity u_∞ = 5 m/s, at the operating outlet pressure Pe = 9 MPa

5.2 Thermal deterioration

Fig. 7 shows the evolution of the wall temperature T_w and bulk temperature T_b as a function of position along the x-axis for different constant heat fluxes and velocities at an operating pressure Pe of 9 MPa.

At low velocity (u_∞ = 5 m/s) and high heat flux (q'' = 5 MW/m²), it is observed that the wall temperature T_w of the square channel increases drastically from the position 0.05 m along the x-axis, reaching a value of 3.6 times the pseudocritical temperature (Tpc = 214 K) at the outlet of the channel.

This increase is consistent with previous research on the conditions for the appearance of the thermal deterioration, which occurs when the fluid temperature near the wall is higher than the pseudocritical temperature, while the bulk temperature defined below is lower.

The bulk temperature is defined by the following relation:

$$T_b = \frac{\int_A \rho\, u\, C_p\, T\, dA}{\int_A \rho\, u\, C_p\, dA} \tag{7}$$

Note that the bulk temperature is almost identical for the rectangular and square channels for a given constant heat flux and inlet velocity.

It increases with increasing heat flux, but it always remains below the pseudocritical temperature.

The same figure (Fig. 7), shows that this drastic increase in temperature is not observed with the rectangular channel under the same conditions.

This again indicates that the rectangular channel is more efficient for supercritical heat transfer and delays the onset of thermal deterioration.

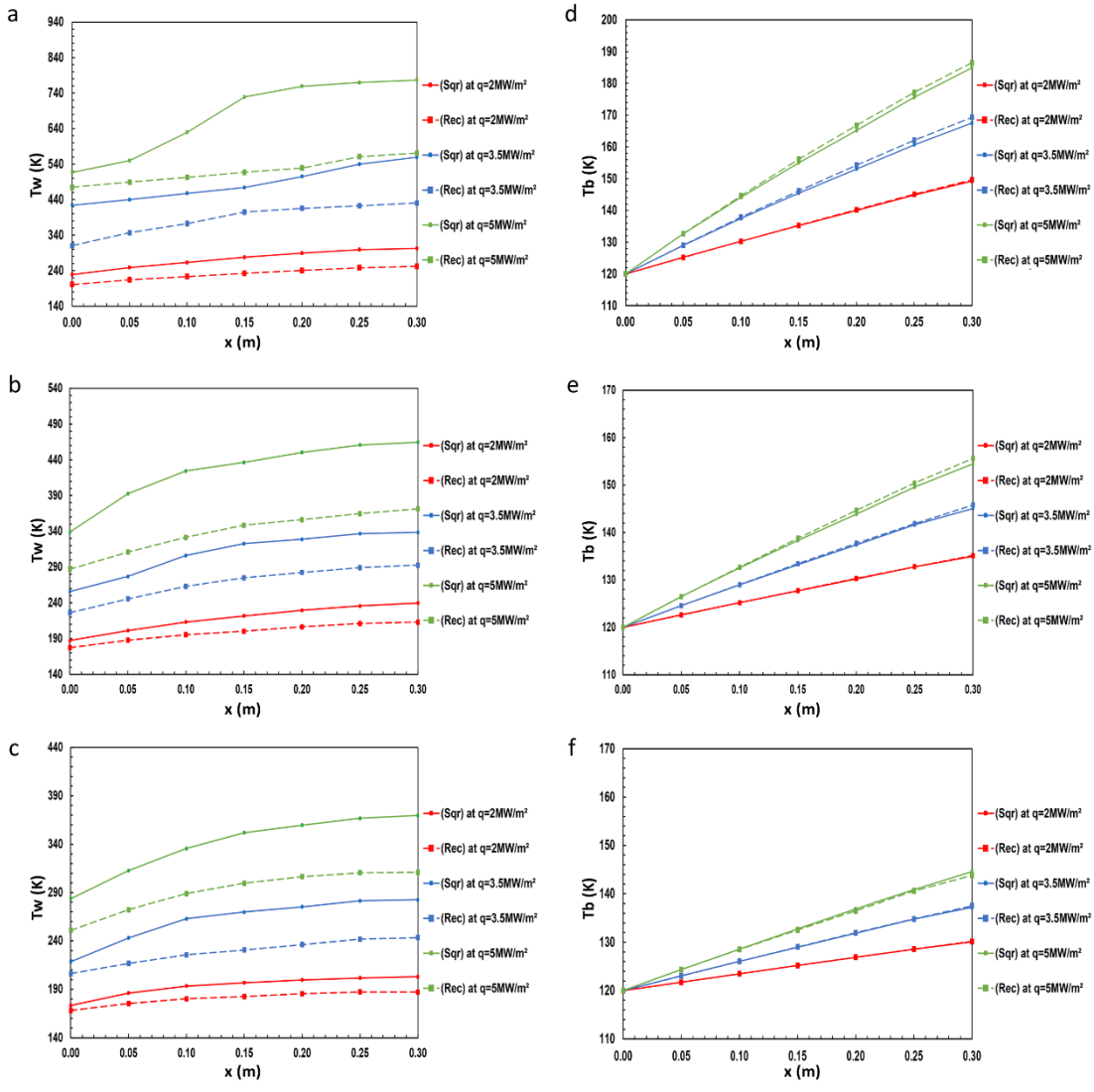

Fig. 7 - At operating pressure *Pe* at 9 MPa: (a), (b) and (c) Variations of wall temperature T_w. (d), (e) and (f) Variations of the bulk temperature T_b. at different heat fluxes, with: (a and d) at u_∞ = 5 m/s, (b and e) at u_∞ = 10 m/s and (c and f) at u_∞ = 15 m/s.

5.3 Pressure losses

The first observation as shown in Table 2 is that by increasing the fluid velocity in channels, the heat transfer efficiency is improved, the temperatures decrease, and the absence of signs of thermal degradation is noted.

However, this increase in velocity also leads to an increase in pressure losses. As an example, for an operating pressure *Pe* = 9 MPa and a heat flux q'' = 5 MW/m², an increase in inlet velocity from 5 m/s to 15 m/s leads to an increase of 450% in pressure losses in a rectangular channel. The second observation is that pressure losses are higher in a rectangular channel than in a square channel.

Indeed, for the same conditions as previously, i.e. operating pressure *Pe* = 9 MPa and a heat flux of q'' = 5 MW/m², there is an increase of 37.5% in pressure losses between the square channel and the rectangular channel for an inlet velocity u_∞ = 15 m/s.

It is worth noting that pressure losses can be more significant with other channel sizes, other boundary conditions, and when taking into account the convergent-divergent shape of the nozzle and its length.

Table 2 - Maximum wall temperature T_{wg} and T_{wa}, and pressure losses at different constant heat fluxes, inlet velocities and operating pressures:

Boundary conditions		**q'' = 2 MW/m²**		**q'' = 3.5 MW/m²**		**q'' = 5 MW/m²**	
		(Sqr)	(Rec)	(Sqr)	(Rec)	(Sqr)	(Rec)
Pe = 9MPa u_∞= 5 m/s	T_{wg} Max (K) :	302.98	252.09	559.34	431.53	776.41	574.35
	T_{wa} Max (K) :	255.16	213.32	485.13	363.35	661.25	471.88
	ΔP (MPa) :	0.005	0.011	0.007	0.012	0.010	0.012
Pe = 9MPa u_∞= 10 m/s	T_{wg} Max (K) :	239.70	213.54	339.37	293.58	465.56	371.96
	T_{wa} Max (K) :	195.46	175.94	262.83	227.18	355.34	277.65
	ΔP (MPa) :	0.021	0.029	0.022	0.029	0.024	0.031
Pe = 9MPa u_∞= 15 m/s	T_{wg} Max (K) :	203.61	187.91	282.69	244.14	370.30	312.90
	T_{wa} Max (K) :	163.46	152.40	207.26	179.57	265.32	218.43
	ΔP (MPa) :	0.045	0.060	0.047	0.065	0.048	0.066
Pe = 6MPa u_∞= 15 m/s	T_{wg} Max (K) :	208.82	193.88	288.59	256.36	374.83	318.87
	T_{wa} Max (K) :	167.64	157.46	215.14	191.60	265.47	228.83
	ΔP (MPa) :	0.042	0.055	0.046	0.055	0.047	0.063
Pe = 12MPa u_∞= 15 m/s	T_{wg} Max (K) :	201.92	187.92	272.04	238.28	356.88	304.68
	T_{wa} Max (K) :	162.45	152.86	198.51	175.36	250.50	210.12
	ΔP (MPa) :	0.045	0.059	0.049	0.066	0.050	0.067

5.4 Effect of operating pressure

In this part of the study, we fixed the inlet velocity u_∞ at 15 m/s and studied the effect of operating pressure on heat transfer, at Pe = 6, 9 and 12 MPa, for the same constant heat fluxes as before. The results of the impact of the change of the operating pressure on the maximum wall temperatures T_{wg} is also shown in Table 2.

We found that operating pressure plays a role in heat transfer. Indeed, we noticed that wall temperatures decrease with increasing pressure.

For example, for the square channel with a heat flux q'' of 5 MW/m², the temperature decreases by 5% between an operating pressure Pe of 6 MPa and 12 MPa.

This observation is consistent with previous research on this topic, and in some of these studies the effect of operating pressure was more significant on heat transfer, such as the study by Bo Ruan and Hua Meng [16].

6. CONCLUSIONS

This paper presents a comparative study of supercritical heat transfer in a regeneratively cooled rocket engine, using three-dimensional numerical simulations for two channel geometries: rectangular and square. The following conclusions could be drawn:

• A rectangular channel is more efficient in terms of heat transfer than a square channel with its high aspect ratio, with a more pronounced difference at high heat fluxes and low velocities.

• Thermal degradation also occurs with high heat fluxes and low velocities, when the methane temperature near the wall is higher than the pseudocritical temperature, while the bulk temperature is lower.

• The rectangular channel delays the onset of thermal deterioration, but despite these advantages in terms of heat transfer efficiency and the advantage of having low wall temperatures compared to the square channel, it has higher pressure losses than the square channel.

Therefore, for applications requiring high heat flux, high inlet velocities are preferable as well as a rectangular channel with a high aspect ratio. However, it is important to consider the associated additional pressure losses.

• Operating pressure also plays a role in improving heat transfer, so as it increases, the maximum wall temperatures decrease.

REFERENCES

[1] H S Mukunda, *Understanding Aerospace Chemical Propulsion*. IK International Publishing House Pvt. Limited, 9789385909429, 2017. [Online]. Available: https://www.abebooks.com/Understanding-Aerospace-Chemical-Propulsion-Mukunda-I.K/21937896504/bd

[2] B. N. Bhat, Editor, *Aerospace Materials and Applications*. Reston ,VA: American Institute of Aeronautics and Astronautics, Inc., 2018, doi: 10.2514/4.104893

[3] M. Arun, J. Akhil, K. Noufal, R. Baby, D. Babu, and M. Jose Prakash, Effect of aspect ratio on supercritical heat transfer of cryogenic methane in rocket engine cooling channels, *Frontiers in Heat and Mass Transfer*, vol. **8**, 2017, 21518629, doi: 10.5098/hmt.8.23

[4] M. F. Wadel and M. L. Meyer, Validation of high aspect ratio cooling in a 89 kN (20,000 lbf) thrust combustion chamber, in *32nd Joint Propulsion Conference and Exhibit*, 1996, p. 2584, doi: 10.2514/6.1996-2584

[5] M. F. Wadel, Comparison of high aspect ratio cooling channel designs for a rocket combustion chamber, in *33rd Joint Propulsion Conference and Exhibit*, National Aeronautics and Space Administration, Lewis Research Center, 1997, doi: 10.2514/6.1997-2913

[6] J. A. Carlile and R. J. Quentmeyer, An experimental investigation of high-aspect-ratio cooling passages, in *AIAA/ASME/SAE/ASEE 28th Joint Propulsion Conference and Exhibit, 1992*, 1992, p. 3154, doi: 10.2514/6.1992-3154

[7] A. Ulas and E. Boysan, Numerical analysis of regenerative cooling in liquid propellant rocket engines, *Aerospace Science and Technology*, vol. **24**, no. 1, pp. 187–197, 2013, 12709638, doi: 10.1016/j.ast.2011.11.006

[8] M. K. and P. M. Thomas Brown, Foundational Methane Propulsion Related Technology Efforts , and Challenges for Applications to Human Exploration Beyond Earth Orbit, *Proceedings of Space Propulsion Conference 2016*, no. May, 2016, doi: 20160006972

[9] G. P. Sutton and H. S. Seifert, Rocket Propulsion Elements, *Physics Today*, vol. **3**, no. 2, pp. 31–32, 1950, 0031-9228, doi: 10.1063/1.3066790

[10] A. Mereu and D. Isvoranu, Joint design and simulation of GOX-GCH4 combustion and cooling in an experimental water-cooled subscale rocket engine, *INCAS Bulletin*, vol. **15**, no. 4, pp. 159–167, 2023, 2066-8201, doi: 10.13111/2066-8201.2023.15.4.13

[11] M. B. Sharabi, W. Ambrosini, and S. He, Prediction of unstable behaviour in a heated channel with water at supercritical pressure by CFD models, *Annals of Nuclear Energy*, vol. **35**, no. 5, pp. 767–782, 2008, 03064549, doi: 10.1016/j.anucene.2007.09.019

[12] X. L. Huai, S. Koyama, and T. S. Zhao, An experimental study of flow and heat transfer of supercritical carbon

dioxide in multi-port mini channels under cooling conditions, *Chemical Engineering Science*, vol. **60**, no. 12, pp. 3337–3345, 2005, 00092509, doi: 10.1016/j.ces.2005.02.039

[13] G. Dang, F. Zhong, Y. Zhang, and X. Zhang, Numerical study of heat transfer deterioration of turbulent supercritical kerosene flow in heated circular tube, *International Journal of Heat and Mass Transfer*, vol. **85**, pp. 1003–1011, 2015, 00179310, doi: 10.1016/j.ijheatmasstransfer.2015.02.052

[14] B. A. Younglove and J. F. Ely, Thermophysical Properties of Fluids. II. Methane, Ethane, Propane, Isobutane, and Normal Butane, *Journal of Physical and Chemical Reference Data*, vol. **16**, no. 4, pp. 577–798, 1987, 15297845, doi: 10.1063/1.555785

[15] Y. Z. Wang, Y. X. Hua, and H. Meng, Numerical studies of supercritical turbulent convective heat transfer of cryogenic-propellant methane, *Journal of Thermophysics and Heat Transfer*, vol. **24**, no. 3, pp. 490–500, 2010, 15336808, doi: 10.2514/1.46769

[16] B. Ruan and H. Meng, Supercritical heat transfer of cryogenic-propellant methane in rectangular engine cooling channels, *Journal of Thermophysics and Heat Transfer*, vol. **26**, no. 2, pp. 313–321, 2012, 15336808, doi: 10.2514/1.T3670

[17] A. A. Bishop, R. O. Sandberg, and L. S. Tong, Forced Convection Heat Transfer to Water at Near-Critical Temperatures and Supercritical Pressures, in *Chemical Engineering under Extreme Conditions, Proceedings of the A.I. Ch.E.-I. Chem.E, Symposium. Series No. 2*, Westinghouse Electric Corp., Pittsburgh, Pa. Atomic Power Div., 1965, pp. 77–85.

[18] H. Gu, H. Li, H. Wang, and Y. Luo, Experimental investigation on convective heat transfer from a horizontal miniature tube to methane at supercritical pressures, *Applied Thermal Engineering*, vol. **58**, no. 1–2, pp. 490–498, 2013, 13594311, doi: 10.1016/j.applthermaleng.2013.04.049

[19] M. Pizzarelli and F. Battista, Oxygen–methane rocket thrust chambers: Review of heat transfer experimental studies, *Acta Astronautica*, vol. **209**. Elsevier, pp. 48–66, 2023. 00945765, doi: 10.1016/j.actaastro.2023.04.028

[20] E. W. Lemmon, I. H. Bell, M. L. Huber, and M. O. McLinden, *Thermophysical Properties of Fluid Systems*. National Institute of Standards and Technology, 2023.

[21] N. J. Simon, E. S. Drexler, R. P. Reed, R. M. White, and J. W. Lyons, *Properties of Copper and Copper Alloys at Cryogenic Temperatures Technology Admlnletndlon*, 1992.

[22] B. Zina, A. Filali, N. Benamara, S. Laouedj, and H. Ahmed, Numerical simulation of heat transfer improvement of a new designed artificially roughened solar air heater using triangular ribs with semi-circular nooks, *Energy Sources, Part A: Recovery, Utilization and Environmental Effects*, pp. 1–17, 2020, 15567230, doi: 10.1080/15567036.2020.1825564

[23] D. Lahmer, N. Benamara, H. Ahmad, H. Ameur, and A. Boulenouar, Combination of the Parallel/Counter Flows Nanofluid Techniques to Improve the Performances of Double-Tube Thermal Exchangers, *Arabian Journal for Science and Engineering*, vol. **47**, no. 6, pp. 7789–7796, 2022, 21914281, doi: 10.1007/s13369-022-06670-3

[24] R. Shaheed, A. Mohammadian, and H. Kheirkhah Gildeh, A comparison of standard k–ε and realizable k–ε turbulence models in curved and confluent channels, *Environmental Fluid Mechanics*, vol. **19**, no. 2, pp. 543–568, 2019, 15731510, doi: 10.1007/s10652-018-9637-1